ECLÉTICA QUÍMICA

Eclet. Quim. 51 | e-1560, 2026

Original Articles in Chemistry and Related Areas

https://doi.org/10.26850/1678-4618.eq.v51.2026.e1560

Synthesis, DFT, molecular docking, and insecticidal activities of 4-aminoantipyrine Schiff bases

Ehimen Annastasia **Erazua**[1+], Babatunde Benjamin **Adeleke**[1]

Abstract

The insecticidal potential of 4-aminoantipyrine derivatives remain underexplored despite their broad scientific applications. To develop safer insecticides for stored grain protection, a series of 4-aminoantipyrine Schiff bases were synthesized and characterized using FTIR, UV-Vis, EI-MS, and ^{1}H NMR spectroscopy. Insecticidal activity against *Tribolium castaneum*, *Sitophilus oryzae*, and *Rhyzopertha dominica* was evaluated via the impregnated filter paper method. Cytotoxicity was assessed using the brine shrimp lethality test. Chemical reactivity descriptors were obtained through Density Functional Theory (DFT), while binding affinities and receptor interactions were investigated using molecular docking simulations with two target receptors. Compounds D, F, and M exhibited excellent insecticidal activity against *Rhyzopertha dominica* at 239.5 µg/cm², while H and K showed moderate effects. None of the synthesized compounds showed activity against *Tribolium castaneum* or *Sitophilus oryzae*. All the synthesized compounds were non-cytotoxic to regular cell lines. These findings highlight D, F, and M as promising leads for the development of next-generation grain storage pesticides.

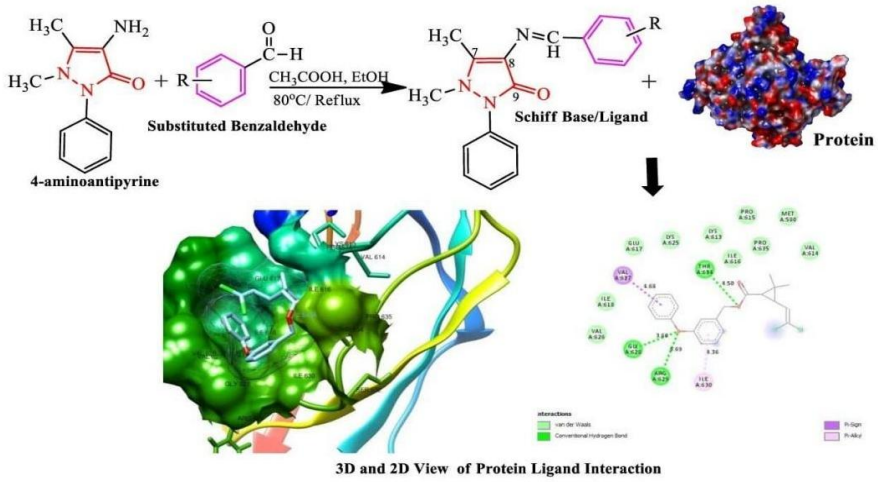

3D and 2D View of Protein Ligand Interaction

Article History

Received May 08, 2024
Accepted May 28, 2025
Published June 15, 2026

Keywords

1. 4-aminoantipyrine
2. insecticidal activity
3. density functional theory
4. *Rhyzopertha dominica*
5. molecular docking

Section Editors

Marcos Carlos de **Mattos**
Rogéria Rocha **Gonçalves**

Highlights

- The design of new 4-aminoantipyrine Schiff bases offers safer insecticides.
- Spectroscopic techniques were used to characterize a series of novel Schiff bases.
- DFT and molecular docking correlated electronic properties with biological activity.
- Compounds D, F, and M showed 100% mortality against *Rhyzopertha dominica*.
- The most active compounds promise a new pesticides generation for gaining storage.

[1]University of Ibadan, Department of Chemistry, Ibadan, Nigeria. **+Corresponding author:** Ehimen Annastasia Erazua, **Phone:** +2347032431289, **Email address:** erazuaann@gmail.com

https://doi.org/10.26850/1678-4618.eq.v51.2026.e1560

1. Introduction

The storage of grains is challenging due to pests and food contamination. Interactions between insects, microorganisms, and grains in silos cause financial losses and mycotoxin accumulation (Herrera *et al.,* 2015). Preserving grain quality is a global priority. Insect damage during storage can lead to losses of 5-10% in industrialized nations and 20-40% in developing nations (Nopsa *et al.,* 2015). Various insect species damage stored food, with over half belonging to the Coleoptera order, accounting for 60% of the total. One such species is *Rhyzopertha dominica,* also known as the Lesser grain borer or grain weevil. This insect can be found in food processing facilities, grain stores, and livestock feed processing facilities. Both adults and larvae of *Rhyzopertha dominica* feed on seeds and grains, including cereal grains like wheat, corn, rice, sorghum, as well as nuts and legumes (Dissanayaka *et al.,* 2020)

Crop protection through chemical control is commonly used due to its effectiveness and accessibility. However, the depletion of ozone caused by certain synthetic pesticides like methyl bromide has led to their discontinuation (Gareau, 2015; Suthisut *et al.,* 2011). In addition, the development of resistant strains by insects, the toxic nature of most insecticides, environmental pollution, toxicity to mammals, disruption of ecological balance, and high costs (Grewal *et al.,* 2017; Khan *et al.,* 2019; Lampiri *et al.,* 2019; Rouhani *et al.,* 2019) have highlighted the need for alternative, non-toxic insecticides to manage pest infestations in stored grains.

The Pyrazole ring is found in some pesticides used in the agrochemical industry, such as fenpyroximate, furametpyr (Kim *et al.,* 2006), tebufenpyrad (Marcic 2005), tolfenpyrad (Nonaka *et al.,* 2003), cyantraniliprole (Selby *et al.,* 2013), and cyenopyrafen (Yu *et al.,* 2012). Inspired by tebufenpyrad and tolfenpyrad, researchers have synthesized pyrazole-related compounds and tested their efficacy against different insects (Halim *et al.,* 2020; Huang *et al.,* 2012; Song *et al.,* 2012; Yaman and Simsek, 2021). 4-aminoantipyrine and its derivatives have various applications in medicine and industry. They possess antibacterial (Singh *et al.,* 2020), anti-inflammatory, analgesic, antipyretic (Murtaza *et al.,* 2017), antifungal (Sabaa *et al.,* 2010), antitumor (Ghorab *et al.,* 2014), and antioxidant (Teran *et al.,* 2019) properties. Recently, their use in areas like corrosion inhibition (Kashyap *et al.,* 2018), catalysis, and metal complexes (Raman *et al.,* 2017) has been explored. However, their application as agrochemicals, especially in pest control, is limited in the literature, and their use against *Rhyzopertha dominica* has not been reported.

In parallel with chemical synthesis and biological evaluation, theoretical methods have become essential in modern pesticide research. Density Functional Theory (DFT) and molecular docking are widely used to predict the electronic reactivity of compounds and their ability to interact with target proteins (Oyebamiji *et al.*, 2021; Zaater *et al.*, 2016).These computational approaches enhance the understanding of structure-activity relationships and provide mechanistic insight into bioactivity, thereby supporting the design of selective, potent, and environmentally safer insecticidal agents (Matsuzaka and Uesawa 2023). DFT is a computational tool used to calculate the structural characteristics of molecular systems, replicating experimental values for chemical descriptors (Kaya *et al.*, 2016). Molecular docking is another computational chemistry tool that predicts the binding affinity between a receptor and a ligand, facilitating their molecular interaction (Huang *et al.*, 2010).

This current study describes the synthesis of some 4-aminoantipyrine Schiff bases and characterization using FT-IR, UV-Vis, EI-MS, and ^{1}H NMR. The synthesized Schiff bases were evaluated for cytotoxicity and insecticidal activities. A detailed study was done using DFT and molecular docking simulation to generate theoretical data to complement the experimental data.

2. Experimental

Solvents and reagents were purchased from suppliers. Melting points (Mp) were measured with a Buchi M-560. IR spectra (υ, cm^{-1}) were recorded with potassium bromide (KBr) disks on Brucker Vector 22 and FTIR-8900 (Shimadzu, Japan) in the range of 4000 to 400 cm^{-1}. The wavelength of maximum absorption (λ_{max}) was obtained using a Thermo Scientific Evolution 300 UV-Vis spectrophotometer in a chloroform solution. Mass-to-charge ratios (m/e) of ions produced were determined by EI-MS using a Jeol-600H-1. ^{1}H-NMR spectra were acquired at 400 MHz and 500 MHz on Bruker Advance spectrometers in DMSO-d_6 and MeOD-d_6. The internal standard utilized was tetramethyl silane (TMS), and the chemical shift values were expressed in parts per million (ppm). The terms singlet, doublet, triplet, quartet, and multiplets are represented by the acronyms s, d, t, q, and m, respectively. Thin layer chromatography (TLC) was used to track the reactions and observed under UV light (254/365 nm).

2.1. Synthesis of 4-aminoantipyrine Schiff bases

The Schiff bases (A-M) were synthesized according to **Scheme 1**, by the condensation of commercially available 4-amino antipyrine with substituted benzaldehyde (**Table 1**) (Murtaza *et al.,* 2017; Teran *et al.,* 2019), Equimolar amounts of 4-aminoantipyrine and benzaldehyde (5 mmol) were heated in 10 mL of ethanol, in a water bath at 80-85 °C for 4-12 h. Glacial acetic acid was used as the catalyst. TLC was used to monitor the reaction's development. Following the completion of the reaction, the precipitates were filtered, recrystallized, and vacuum dried. The products obtained were elucidated with ^{1}H-NMR, EI-MS, UV- Visible and FT-IR spectroscopy.

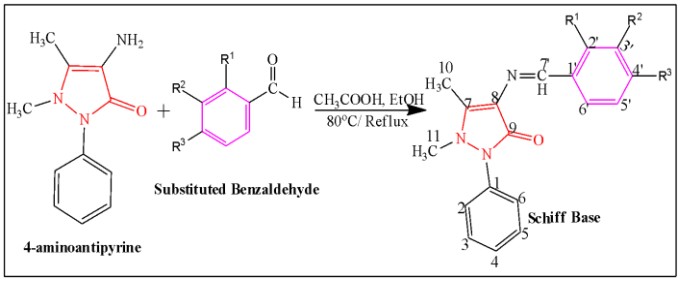

Scheme 1. Synthetic route for 4-aminoantipyrine Schiff bases.
Note: **R1**, **R2**, and **R3** = different substituents on benzaldehyde.
Source: Elaborated by the authors.

Table 1. Description of the substituents on Schiff bases.

Compound	Molecular Formula	R^1	R^2	R^3
A	$C_{18}H_{17}N_3O$	H	H	H
B	$C_{18}H_{16}FN_3O$	H	H	F
C	$C_{18}H_{16}FN_3O$	F	H	H
D	$C_{18}H_{16}ClN_3$	H	H	Cl
E	$C_{18}H_{16}ClN_3$	Cl	H	H
F	$C_{18}H_{16}BrN_3O$	H	H	Br
G	$C_{18}H_{16}BrN_3O$	Br	H	H
H	$C_{19}H_{19}N_3O_3$	H	OCH_3	OH
I	$C_{19}H_{19}N_3O_3$	OH	OCH_3	H
J	$C_{19}H_{19}N_3O_3$	H	OH	OCH_3
K	$C_{19}H_{19}N_3O$	H	H	CH_3
L	$C_{18}H_{17}N_3O_3$	H	OH	OH
M	$C_{18}H_{17}N_3O_3$	OH	H	OH

Source: Elaborated by the authors.

2.2. Evaluation of cytotoxicity using brine shrimp lethality assay

The Brine shrimp lethality assay is a preliminary screening technique used for determining the cytotoxicity of synthesized compounds. This test was conducted as described in the literature (Banti and Hadjikakou, 2010; Suryawanshi *et al.,* 2020). Brine shrimp eggs weighing 50 mg were sprinkled into the hatching tray, which was half-filled with brine solution. This was incubated at 37 ºC, and the eggs hatched into larvae within two days. The test sample contained 20 mg of the compounds in 2 mL of DMSO. Concentrations of 10, 100, and 1000 µg/mL were obtained using 5, 50, and 500 µL of the test sample, respectively. After 48 h of hatching and developing into nauplii, 10 larvae were placed per vial, and 5 mL of seawater was added. Each vial was placed in the incubator under illumination at 25-27º C for twenty-four hours. The reference drug, etoposide, served as the positive control, and the solvent was the negative control. The Finney computer program was used to analyse the data to determine the percentage mortality with 95% confidence intervals.

2.3. Evaluation of insecticidal activity

Insecticidal activities of the Schiff bases against three insect species (*Tribolium castaneum*, *Sitophilus oryzae* and *Rhyzopertha dominica*) were evaluated by using the impregnated filter paper method (Neggaz *et al.,* 2010). The stored grain pests utilized in this experiment were raised in plastic bottles containing sterile breeding material in a laboratory setting with controlled temperature and humidity levels (25-35 °C and 50-70%). Healthy and active insects of the same size and age were employed. To develop the test samples, add 3 mL of volatile solvent to 20 mg of pure synthesized compounds. The filter paper was placed on the petri plate, the test samples were loaded on it, and this was allowed to evaporate completely for 24 h. Each plate contained 10 insects of the same species. The plates were incubated for twenty-four hours in a growth chamber at a temperature of 27 °C. After 24 h, the insects that were alive were counted and the percentage mortality was calculated as shown in **Eq. 1**. The positive control contains Permethrin (standard insecticide) and the test insect, while the negative control contains the test insect. The solvent concentration of the test sample and standard drug was 239.5 µg/cm^2.

$$\text{Percentage mortality} = 100 - \frac{Number\ \ of\ \ living\ insects\ in\ test\ compounds}{Number\ of\ living\ insect\ in\ control}\ X\ 100 \quad (1)$$

2.4. Computational studies (optimization, DFT and molecular docking)

Five of the synthesized compounds that showed activities against *Rhyzopertha dominica* were selected for theoretical studies. The molecular structure of these compounds was drawn and minimized using Spartan 14 software to obtain the least amount of energy and stable conformation. The strain energy was eliminated from the molecule using a molecular mechanic force field. DFT was used to execute the optimization in a vacuum using the 6-31+G* (d, p) as the basis set, which includes Becke's gradient exchange-correlation, and the Lee-Yang Parr correlation functional (i.e., B3LYP) (Becke, 1993; Yang *et al.,* 2005). The energy difference known as the electronic gap was obtained as the difference between the energy of the lowest unoccupied molecular orbital (E_{LUMO}) and the energy of the highest occupied molecular orbital E_{HOMO}.

Molecular docking was utilized to examine the most likely mode of interaction between the examined compounds (ligands) and the target. PDB ID: 3WE1 and PDB ID: 5B1C downloaded from the database of proteins (www.rcsb.org) were the target used for the modelling. The synthesized compounds, which are potential inhibitors of *Rhyzopertha dominica,* were used as ligands. The proteins were prepared using Chimera 1.14 by removing multiple ligands, water molecules, and other foreign compounds downloaded together with the proteins. The ligands and prepared proteins were converted to PDBQT format with the aid of Autodock 4.2. from PyRX. Grid space was set to dimensions of x = 7.142 nm, y = 5.355 nm, z = 2.480 nm, and size x = 3.845 nm, y = 4.119 nm, z = 4.746 nm were for 3WE1. Grid size of x = 4.545 nm, y = 3.170 nm, z = 4.884 nm and dimensions x = –2.492 nm, y = 4.723 nm, z = 0.373 nm were set for 5B1C. Docking was done with Autodock Vina via PyRX workspace (Trott and Olson, 2010) and the binding energy (kJ/mol) was obtained. Finally, the protein-ligand complex was viewed in 3D using UCSF Chimera 1.14, while the chemical interactions were visualized in 2D using Discovery Studio 2020. The best poses were screened by examination of binding energy (**Eq. 2**), and the molecular interaction of both hydrophobic and hydrophilic types for each complex was observed. The inhibition constants *Ki* were calculated according to the **Eq. 3** (Yusuf *et al.,* 2020).

$$\Delta G = -RTInKi \quad (2)$$

$$\text{Inhibition constant } Ki = exp\ (\Delta G/RT) \quad (3)$$

where ΔG = binding affinity in kJ/mol, R = gas constant (0.008314 kJ/mol/K), T = 298.15 K, *Ki* = Inhibition constant (µ/M).

https://doi.org/10.26850/1678-4618.eq.v51.2026.e1560

3. Results and discussions

The physical data obtained and the percentage mortality of the synthesized compounds are displayed in **Table 2**.

The Schiff bases were prepared as shown in **Scheme 1**. All synthesized compounds were obtained in good yield. **Table 2** displays the physical data obtained and the percentage mortality of the synthesized compounds. The chemical structures of the synthesized compounds were characterized using a variety of spectroscopic techniques. Brine shrimp lethality test was employed in the screening of the compounds for cytotoxicity, and it was discovered that they were not cytotoxic to regular cell lines.

FTIR spectra for the synthesized compounds showed vibrational signals at the expected frequencies for the relevant functional moiety. The stretching vibration bands observed at 1569-1598 cm^{-1} showed that C=N (imine bond) is present. This confirms the formation of the compounds, and the values are within the range reported in the literature (Murtaza *et al.,* 2017). The formation of the Schiff bases was further established by the absence of the NH_2 band of primary amines in the region of 3350-3310 cm^{-1}. The UV-visible absorption spectra of the compounds were obtained in chloroform. The compounds showed distinctive broad absorption bands in the UV-Vis range, from 326-347 nm. The UV spectra of the compounds exhibit similarities, indicating a structural similarity between them.

Table 2. Physical data and percentage mobility of synthesized Schiff bases.

S/N	Compound	Colour	MW (g mol^{-1})	MF	Mp °C	Yield (%)	% Mortality
1	A	Cream	291.35	$C_{18}H_{17}N_3O$	176.0-176.8	91	Inactive
2	B	Pale yellow	309.34	$C_{18}H_{16}FN_3O$	232.0-233.3	86	Inactive
3	C	Yellow	309.34	$C_{18}H_{16}FN_3O$	174.9-176.5	92	Inactive
4	D	Pale yellow	325.80	$C_{18}H_{16}ClN_3$	252.3-253.5	90	100
5	E	Pale yellow	325.80	$C_{18}H_{16}ClN_3$	192.1-193.0	92	Inactive
6	F	Pale yellow	370.25	$C_{18}H_{16}BrN_3O$	251.9-252.8	75	100
7	G	Yellow	370.25	$C_{18}H_{16}BrN_3O$	177.3-179.9	88	Inactive
8	H	Pale yellow	337.38	$C_{19}H_{19}N_3O_3$	207.1-208.3	82	70
9	I	Yellow	337.38	$C_{19}H_{19}N_3O_3$	233.1-234.4	89	Inactive
10	J	Pale yellow	337.38	$C_{19}H_{19}N_3O_3$	243.8-244.5	92	Inactive
11	K	Yellow	305.38	$C_{19}H_{19}N_3O$	184.3-184.8	74	50
12	L	Light brown	323.35	$C_{18}H_{17}N_3O_3$	275.9-276.6	91	Inactive
13	M	Yellow	323.35	$C_{18}H_{17}N_3O_3$	229.2-230.0	90	100

Note: MW=Molecular weight; Mp=Melting point; MF=Molecular Formula.
Source: Elaborated by the authors.

The compounds' ^{1}H NMR spectra were captured in DMSO and methanol. The spectra displayed peaks corresponding to aromatic, methyl, and olefinic protons. The sharp singlet shows the azomethine (-N=CH-) proton at about 9.25 to 9.979 ppm, which validates the Schiff bases' formation. The peaks at δ 6.253-8.21 ppm were assigned to aromatic protons (Ar-H). The aromatic protons seen around δ = 8 ppm for some of these compounds are due to the electron-rich species on the benzaldehyde ring's substituents, which increases the protons' chemical shift due to the deshielding effect. The methyl group linked to the nitrogen (N-CH_3) was observed as a sharp singlet at 3.114-3.273 ppm, while the second methyl group attached to carbon was observed at δ 2.399-2.512 ppm. This is because the electronegative nitrogen atom in the N-CH_3 has a greater deshielding effect. EI-MS spectra showed prominent molecular ion peaks, confirming the mass of each molecule. Below is a summary of the compounds' structural elucidation.

1. 4-(benzylideneamino)-1,5-dimethyl-2-phenyl-1,2-dihydro-3H-pyrazol-3-one (A):

Cream crystal; Yield: 91%; Mp: 176.0-176.8 °C; ^{1}HNMR (500 MHz, δ ppm MeOD-d_6): 9.54 (s, 1H, $H_{7'}$, N=CH), 7.831 (dd, *J* = 8, 1.5 Hz, 2H, $H_{2',6'}$ Ar-H), 7.574 (t, *J*= 7.5, 1.5 Hz, 2H, $H_{3,5}$ Ar-H), 7.467 (t, *J* = 7.5, 1.5 Hz, 1H, $H_{4'}$ Ar-H), 7.440 (t, *J*= 1.5 Hz, 1H, H_4, Ar-H), 7.420 (d, *J*= 2.5 Hz, 2H, $H_{2,6}$ Ar-H) 7.410 (d, *J*= 6.5 Hz, 2H, $H_{3',5'}$ Ar-H), 3.247 (s, 3H, H_{11}, N-CH_3) and 2.512 (s, 3H, H_{10}, CH_3). EI-MS (m/z): 291 [M^++1]. FT-IR (cm^{-1}): 3043 (C-H Ar), 2936 (C-H CH_3), 1643 (C=O), 1594 (C=N), 1564 (C=C), 1305 (C-N) and 1211 (N-N); UV (λ_{max}, $CHCl_3$): 326 nm.

2. 4-((4-fluorobenzylidene)amino)-1,5-dimethyl-2-phenyl-1,2-dihydro-3H-pyrazol-3-one (B):

Pale Yellow crystal; Yield: 86%; Mp: 232.0-233.3 °C; ^{1}HNMR (500 MHz, δ ppm, DMSO-d_6): 9.798 (s, 1H, $H_{7'}$, N=CH), 8.188 (d, *J* = 7.2 Hz, 1H, $H_{6'}$ Ar-H), 7.959 (d, *J* = 8 Hz, 1H, $H_{3'}$ Ar-H), 7.785 (t, *J*= 8 Hz, 1H, $H_{5'}$ Ar-H), 7.647 (dd, *J*= 7.2, 2 Hz, 1H, $H_{4'}$ Ar-H), 7.551 (t, *J* = 8 Hz, 2H, $H_{3,5}$ Ar-H), 7.411 (d, *J* = 7.6 Hz, 1H, H_4 Ar-H), 7.372 (d, *J* = 7.6 Hz, 2H, $H_{2,6}$ Ar-H) 3.230 (s, 3H, H_{11}, N-CH_3) and 2.450 (s, 3H, H_{10}, CH_3). EI-MS (m/z) 309 [M^++1]. FT-IR (cm^{-1}): 3069 (C-H Ar), 2937 (C-H CH_3), 1651 (C=O), 1598 (C=N), 1567 (C=C), 1304 (C-N), 1220 (N-N). UV (λ_{max}, $CHCl_3$): 327 nm.

3. 4-((2-fluorobenzylidene)amino)-1,5-dimethyl-2-phenyl-1,2-dihydro-3H-pyrazol-3-one (C):

Yellow crystal; Yield: 92 %; Mp: 174.9-176.5 °C; ^{1}HNMR (500 MHz, δ ppm, MeOD-d_6): 9.808 (s, 1H, $H_{7'}$, N=CH), 8.149 (dd, *J* = 7.5, 2 Hz, 1H, $H_{6'}$ Ar-H), 7.573 (dd, *J* = 7.5, 2 Hz, 2H, $H_{3,5}$ Ar-H), 7.470 (dd, *J* = 8.5, 1.5 Hz, 1H, $H_{4'}$ Ar-H), 7.398 (d, *J* = 3 Hz, 1H, H_4 Ar-H), 7.246 (t, *J* = 7.5 Hz, 1H, $H_{5'}$ Ar-H), 7.149 (dd, *J* = 7.5, 1.5 Hz, 1H, H-3' Ar-H), 3.265 (s, 3H, H_{11}, N-CH_3) and 2.523 (s, 3H, H_{10}, CH_3). EI-MS (m/z) 309 [M^++1]. FT-IR $\bar{\upsilon}$ (cm^{-1}): 3057 (C-H Ar), 2938 (C-H CH_3), 1649 (C=O), 1570 (C=N), 1487 (C=C), 1305 (C-N) and 1229 (N-N). UV (λ_{max}, $CHCl_3$): 329 nm.

4. (Z)-4-((4-chlorobenzylidene)amino)-1,5-dimethyl-2-phenyl-1,2-dihydro-3H-pyrazol-3-one (D):

Pale Yellow crystal; Yield: 90 %; Mp: 252.3-253.5 °C; ^{1}HNMR (500 MHz, δ ppm, DMSO-d_6: 9.550 (s, 1H, $H_{7'}$, N=CH), 7.827 (d, *J* = 8.5 Hz, 2H, $H_{2',6'}$ Ar-H), 7.539 (d, *J*= 8.5 Hz, 2H, $H_{3',5'}$ Ar-H), 7.509 (d, *J*= 8.5 Hz, 2H, $H_{3,5}$ Ar-H), 7.387 (dd, *J*= 8, 1 Hz, 2H, $H_{2,6}$ Ar-H), 7.371 (d, *J* = 7.5 Hz,1H, H_4 Ar-H), 3.183 (s, 3H, H_{11}, N-CH_3) and 2.447 (s, 3H, H_{10}, CH_3). EI-MS (m/z) 325.5 [M^++1]. FT-IR (cm^{-1}): 3060 (C-H Ar), 2936 (C-H CH_3), 1650 (C=O), 1594 (C=N), 1570 (C=C), 1302 (C-N) and 1214 (N-N). UV (λ_{max}, $CHCl_3$): 336 nm.

5. (Z)-4-((2-chlorobenzylidene)amino)-1,5-dimethyl-2-phenyl-1,2-dihydro-3H-pyrazol-3-one (E):

Pale Yellow crystal; Yield: 92 %; Mp: 192.1-193.0 °C; ^{1}HNMR (400 MHz, δppm MeOD-d_6: 9.979 (s, 1H, $H_{7'}$, N=CH), 8.210 (dd, J = 9.6, 1.2 Hz, 1H, $H_{6'}$ Ar-H), 7.575 (t, J = 8, 2 Hz, 2H, $H_{3,5}$ Ar-H), 7.473 (t, J= 7.6, 1.2 Hz, 1H, $H_{4'}$ Ar-H), 7.416 (dd, J = 7.6, 1.6 Hz, 2H, $H_{2,6}$ Ar-H), 7.400 (d, J = 1.2 Hz, 1H, H_4 Ar-H), 7.368 (dd, J = 2.8 Hz, 1H, $H_{3'}$ Ar-H), 7.351 (dd, J = 6.8, 2.8 Hz, 1H, $H_{5'}$ Ar-H), 3.268 (s, 3H, H_{11}, N-CH_3) and 2.525 (s, 3H, H_{10}, CH_3). EI-MS (m/z) 325 [M^++1]. FT-IR (cm^{-1}): 3056 (C-H Ar), 2936 (C-H CH_3), 1648 (C=O), 1589 (C=N), 1562 (C=C), 1305 (C-N) and 1213 (N-N). UV (λ_{max}, $CHCl_3$): 336 nm.

6. 4-((4-bromobenzylidene)amino)-1,5-dimethyl-2-phenyl-1,2-dihydro-3H-pyrazol-3-one (F):

Pale yellow crystal; Yield: 75 %; Mp: 251.9-252.8 °C; ^{1}HNMR (500 MHz, δ ppm DMSO-d_6): 9.535 (s, 1H, $H_{7'}$, N=CH), 7.756 (d, J = 8.5 Hz, 2H, $H_{2',6'}$ Ar-H), 7.646 (d, J= 8.5 Hz, 2H, $H_{3',5'}$ Ar-H) 7.539 (t, J = 7.5 Hz, 2H, $H_{3,5}$ Ar-H), 7.387 (d, J = 8.5 Hz, 2H, $H_{2,6}$ Ar-H) and 7.378 (d, J = 7.5 Hz, 1H, H_4 Ar-H), 3.183 (s, 3H, H_{11}, N-CH_3) and 2.445 (s, 3H, H_{10}, CH_3). EI-MS (m/z) 370 [M^++1]. FT-IR (cm^{-1}): 3058 (C-H Ar), 2935 (C-H CH_3), 1649 (C=O), 1593 (C=N), 1569 (C=C), 1302 (C-N) and 1168 (N-N). UV (λ_{max}, $CHCl_3$): 338 nm.

7. 4-((2-bromobenzylidene)amino)-1,5-dimethyl-2-phenyl-1,2-dihydro-3H-pyrazol-3-one (G):

Yellow crystal; Yield: 88 %; Mp:177.3-179.9 °C.^{1}HNMR, (400 MHz, δ ppm, MeOD-d_6): 9.930 (s, 1H, $H_{7'}$, N=CH), 8.192 (dd, J = 8, 1.6 Hz, 1H, H-6' Ar-H), 7.614 (d, J = 8 Hz, 1H, H_3' Ar-H), 7.578 (t, J = 8 Hz, 2H, $H_{3,5}$ Ar-H), 7.472 (t, J = 7.2, 1.6 Hz, 1H, $H_{5'}$ Ar-H), 7.420 (d, J = 1.6 Hz, 1H, H_4 Ar-H), 7.398 (d, J = 7.2 Hz, 2H, $H_{2,6}$ Ar-H), 7.303 (dd, J= 8, 1.2 Hz, 1H, $H_{4'}$ Ar-H), 3.273 (s, 3H, H_{11}, N-CH_3), and 2.527 (s, 3H, H_{10}, CH_3). EI-MS (m/z) 369 [M^+-1]. FT-IR (cm^{-1}): 3061 (C-H Ar), 2928 (C-H CH_3), 1651 (C=O), 1584 (C=N), 1563 (C=C), 1305 (C-N), 1212 (N-N). UV (λ_{max}, $CHCl_3$): 337 nm.

8. 4-((4-hydroxy-3-methoxybenzylidene)amino)-1,5-dimethyl-2-phenyl-1,2-dihydro-3H-pyraz- ol-3-one (H):

Pale yellow crystal; Yield: 82 %; Mp: 207.1-208.3 °C; ^{1}HNMR (500 MHz, δ ppm MeoD-d_6): 9.395 (s, 1H, $H_{7'}$, N=CH), 7.560 (t, J= 7.5 Hz, 2H, $H_{3,5}$ Ar-H), 7.511 (d, J= 2 Hz, 1H, $H_{2'}$ Ar-H), 7.445 (d, J = 7 Hz, 1H, $H_{6'}$ Ar-H) 7.412 (d, J = 8, 1 Hz, 2H, $H_{2,6}$ Ar-H), 7.221 (dd, J= 8, 1.5 Hz, 1H, H_4 Ar-H), 6.845 (d, J = 8 Hz, 1H, $H_{5'}$ Ar-H), 3.913 (s, 3H, $H_{8'}$, OCH_3) 3.203 (s, 3H, H_{11}, N-CH_3) and 2.475 (s, 3H, H_{10}, CH_3). EI-MS (m/z) 337 [M^++1]. FT-IR (cm^{-1}): 3653 (O-H), 3105 (C-H Ar), 2942 (C-H CH_3), 1627 (C=O), 1580 (C=N), 1517 (C=C), 1416 (C-O bend), 1345 (C-N), 1285 (C-O stretch), 1214 (N-N). UV (λ_{max}, $CHCl_3$): 337 nm.

9. 4-((2-hydroxy-3-methoxybenzylidene)amino)-1,5-dimethyl-2-phenyl-1,2-dihydro-3H-pyrazol-3-one (I):

Yellow crystal; Yield: 89 %; Mp: 233.1-234.4 °C; ^{1}HNMR (400 MHz, δ ppm, DMSO-d6): 13.011 (s, 1H, $H_{4'}$, OH), 9.673 (s,1H, N=CH, $H_{7'}$), 7.553 (dt, J = 7.6, 1.6 Hz, 2H, $H_{3,5}$ Ar-H), 7.409 (dd, J = 7.6, 1.2 Hz, 2H, $H_{2,6}$ Ar-H), 7.375 (d, J = 1.2Hz, 1H, H_4 Ar-H), 7.059 (dd, J = 8, 1.2 Hz, 1H, $H_{6'}$ Ar-H), 7.039 (J = 6.8 Hz, 1H, H-$_{4'}$ Ar-H), 6.860 (t, J= 8 Hz,1H, $H_{5'}$ Ar-H), 3.796 (s, 1H, $H_{8'}$, OCH_3). 3.202 (s, 3H, H_{11}, N-CH_3) and 2.399 (s, 3H, H_{10}, CH_3. EI-MS (m/z) 337 [M^++1]. FT-IR (cm^{-1}): 3736 (O-H), 3069 (C-H Ar), 2924 (C-H CH_3), 1664 (C=O), 1593 (C=N), 1487 (C=C), 1419 (C-O bend), 1296 (C-N), 1247 (C-O stretch), 1068 (N-N). UV (λ_{max}, $CHCl_3$): 335 nm.

10. 4-((3-hydroxy-4-methoxybenzylidene)amino)-1,5-dimethyl-2-phenyl-1,2-dihydro-3H-pyrazol-3-one (J):

Pale yellow crystal; Yield: 92 %; Mp: 243.8-244.5 °C; ^{1}HNMR, (500 MHz, δ ppm, MeOD-d_6): 9.388 (s, 1H, $H_{7'}$ N=CH,) 7.565 (dt, J = 7.5, 1.5 Hz, 2H, $H_{3,5}$ Ar-H), 7.454 (dt, J= 2.5Hz, 1H, $H_{2'}$ Ar-H), 7.422 (dd, J = 2 Hz, 1H, H_4 Ar-H), 7.397 (J = 2 Hz, 2H, $H_{2,6}$ Ar-H), 7.214 (dd, J= 8.5, 2 Hz, 1H, $H_{6'}$ Ar-H), 6.980 (d, J = 8.5Hz, 1H, $H_{5'}$ Ar-H) 3.896 (s, 1H, $H_{8'}$, OCH_3), 3.218 (s, 3H, H_{11}, CH_3) and 2.484 (s,3H, H_{10}, CH_3). EI-MS (m/z) 337 [M^++1]. FT-IR (cm^{-1}): 3740 (O-H), 3069 (C-H Ar), 2963 (C-H CH_3), 1615 (C=O), 1568 (C=N), 1519 (C=C), 1425 (C-O bend), 1310 (C-N), 1255 (C-O stretch), 1027 (N-N). UV (λ_{max}, $CHCl_3$): 337 nm.

11. 1,5-dimethyl-4-((4-methylbenzylidene)amino)-2-phenyl-1,2-dihydro-3H-pyrazol-3-one (K):

Yellow crystal; Yield: 74 %; Mp:184.3-184.8 °C; ^{1}HNMR, (500 MHz, δ ppm, MeOD-d6): 9.490 (s, 1H, $H_{7'}$, N=CH), 7.716 (d, J = 8 Hz, 2H, $H_{2',6'}$ Ar-H), 7.568 (t, J = 8, 2 Hz, 2H, $H_{3,5}$ Ar-H), 7.457 (t, J = 7.5 Hz, 1H, H_4 Ar-H), 7.415 (dd, J = 9, 1.5 Hz, 2H, $H_{2,6}$ Ar-H), 7.250 (d, J= 8 Hz, 2H, $H_{3',5'}$ Ar-H), 3.230 (s, 3H, H_{11}, N-CH_3), 2.494 (s, 3H, H_{10}, CH_3) and 2.373 (s, 3H, $H_{8'}$, CH_3). EI-MS (m/z) 305 [M^++1]. FT-IR (cm^{-1}): 3056 (C-H Ar), 2920 (C-H CH_3), 1653 (C=O), 1577 (C=N), 1498 (C=C), 1302 (C-N), 1213 (N-N). UV (λ_{max}, $CHCl_3$): 327 nm.

12. 4-((3,4-dihydroxybenzylidene)amino)-1,5-dimethyl-2-phenyl-1,2-dihydro-3H-pyrazol-3-one (L):

Light brown crystal; Yield: 91 %; Mp: 275.9-276.6 °C; 1HNMR, (500 MHz, δ ppm, DMSO-d_6): 9.370 (s,1H, $H_{7'}$, N=CH) 9.204 (s, 1H, $H_{3'}$, OH), 7.523 (t, J = 8 Hz, 2H, $H_{3,5}$ Ar-H), 7.367 (s, 1H, $H_{2'}$ Ar-H), 7.352 (d, J= 7 Hz, 2H, $H_{2,6}$ Ar-H), 7.287 (d, J = 2 Hz, 1H, $H_{6'}$ Ar-H), 7.020 (dd, J = 8, 2 Hz, 1H, H_4 Ar-H), 6.784 (d, J = 8.5 Hz, 1H, $H_{5'}$ Ar-H), 3.451 (q, 1H, $H_{4'}$ OH), 3.114 (s, 3H, H_{11}, N-CH_3) and 2.400 (s, 3H, H_{10}, CH_3). EI-MS (m/z) 323 [M^++1]. FT-IR (cm^{-1}): 3495 (O-H), 3062 (C-H Ar), 2943 (C-H CH_3), 1616 (C=O), 1589 (C=N), 1561 (C=C), 1377 (C-O bend), 1289 (C-N), 1266 (C-O stretch), 1071 (N-N); UV (nm): UV (λ_{max}, $CHCl_3$): 338 nm.

13. 4-((2,4-dihydroxybenzylidene)amino)-1,5-dimethyl-2-phenyl-1,2-dihydro-3H-pyrazol-3-one (M):

Yellow crystal; Yield: 90 %; M.p: 229.2-230.0 °C; ^{1}HNMR, (500 MHz, δ ppm, DMSO-d_6): 13.307 (s, 1H, $H_{2'}$, O-H), 10.045 (s, 1H, $H_{4'}$, O-H), 9.545 (s, 1H, $H_{7'}$), 7.538 (t, J= 8 Hz, 2H, $H_{3,5}$ Ar-H), 7.381 (dd, J = 6.5, 1.5 Hz, 2H, $H_{2,6}$ Ar-H), 7.370 (d, J_4 = 6.5 Hz, 1H, H_4 Ar-H), 7.245 (d, J = 8.5 Hz, 1H, $H_{6'}$ Ar-H), 6.349 (dd, J = 8, 2 Hz, 1H, $H_{5'}$ Ar-H), 6.253 (d, J = 2 Hz, 1H, $H_{3'}$ Ar-H), 3.148 (s, 3H, H_{11}, N-CH_3), 2.349 (s, 3H, H_{10}, CH_3). EI-MS (m/z) [M^++1]. FT-IR (cm^{-1}): 3450 (O-H), 3059 (C-H Ar), 2921 (C-H CH_3), 1616 (C=O), 1580 (C=N), 1512 (C=C), 1366 (C-O bend), 1318 (C-N), 1225 (C-O stretch), 1160 (N-N). UV (λ_{max}, $CHCl_3$): 347 nm.

3.1. Cytotoxicity activity

The cytotoxicity of the synthesized Schiff bases was evaluated using the *Artemia salina* lethality assay, a well-established, rapid, and cost-effective bioassay widely used for preliminary toxicity screening of bioactive compounds. This model is recognized for its simplicity, reproducibility, and correlation with cytotoxicity in higher organisms, making it a reliable predictor of general toxicity profiles (Banti and Hadjikakou, 2010; Suryawanshi *et al.*, 2020).

In this study, none of the tested compounds exhibited significant lethality at concentrations up to 1000 µg/mL, indicating low acute toxicity. This result suggests that the active

insecticidal compounds, particularly **D**, **F**, and **M**, possess selective toxicity toward *Rhyzopertha dominica* without exhibiting general cytotoxic effects. The lack of cytotoxicity is desirable in pesticide development, as it minimizes the risk to non-target organisms and supports the potential environmental safety of these compounds.

3.2. Insecticidal activity

Insecticidal activities of the compounds against three insect species (*Tribolium castaneum, Sitophilus oryzae and Rhyzopertha dominica*), were evaluated by the impregnated filter paper method using permethrin as standard. Interestingly, insecticidal activities of all the synthesized compounds against these insect species have not been reported. The compounds were found to be active against only one species (*Rhyzopertha dominica*), and the result is displayed in **Table 2**. Five compounds were observed to possess insecticidal activities against *Rhyzopertha dominica*, with compounds **D**, **F**, and **M** having excellent potency (100% inhibition) as the standard used. Compounds **H** and **K** were moderately active (70 and 50 % inhibition, respectively). The structure-activity relationship shows that changing the benzene ring's substituent could result in a striking shift in bioactivity. The compound without a substituent on benzene (compound **A**) showed no activity. The compounds' insecticidal activity increased as the substituents varied at different positions on the benzaldehyde. Hence, the inhibitory strength of the Schiff bases was significantly influenced by the type and position of the substituent.

3.3. Computational studies

Density Functional Theory (DFT) was employed in this study to gain insight into the electronic structure and chemical reactivity of the synthesized 4-aminoantipyrine Schiff bases, which show insecticidal activities. DFT calculations also allowed us to establish structure-activity relationships by correlating electronic properties with insecticidal efficacy. Thus, DFT served as a predictive tool that complemented our experimental findings and supported the identification of promising candidates for further agrochemical development.

The molecular descriptors obtained are shown in **Table 3**. These descriptors are discussed in relation to the compounds' inhibition constant (*Ki*), binding energy (**Tables 4** and **5**), and reactivity. Frontier molecular orbitals (HOMO and LUMO), as well as the electronic gap, are used to explain the electronic properties, stability, reactivity, and bioactivity of a molecule (Erazua and Adeleke, 2019; Erazua *et al.,* 2019; Erazua *et al.,* 2021; Zaater *et al.,* 2016). It has been established that higher $E_{HOMO,}$ lower $E_{LUMO,}$ and a small electronic gap confer the molecule a better ability to interact with other chemical species (Erazua *et al.*, 2024) and result in lower *Ki* values. The E_{LUMO} revealed that compounds **D**, **F** and **M** are more active than the other studied compounds. Compound **M**, with the lowest electronic gap value, possesses a low value of *Ki* (although not the lowest in the study). In contrast, compound **K** with the highest electronic gap, gives the highest value of *Ki* and will have the least interaction with the receptors. This trend is the same for experimental results. Compounds that showed low LUMO energy and narrow electronic gaps, such as **D**, **F**, and **M**, exhibited enhanced insecticidal activity against *Rhyzopertha dominica*. This is consistent with previous studies demonstrating that a small electronic gap often corresponds to increased molecular reactivity and stronger biological interactions (Akbari *et al.,* 2024; Erazua *et al*., 2023; Raza *et al*., 2023).

Table 3. The E_{HOMO}, E_{LUMO}, and electronic gap global reactivity descriptors of the active synthesized compounds.

Molecules	E_{HOMO} (eV)	E_{LUMO} (eV)	Electronic gap (eV)	η (eV)	σ (Ev^{-1})	M (eV)	ω (eV)	χ (eV)
D	−5.55	−1.56	3.99	2.0	0.50	-3.56	3.17	3.56
F	−5.56	−1.58	3.98	1.99	0.50	-3.57	3.2	3.57
H	−5.21	−1.21	4.0	2.0	0.50	-3.21	2.58	3.21
K	−5.35	−1.28	4.07	2.04	0.49	-3.32	2.7	3.32
M	−5.27	−1.33	3.94	1.97	0.51	-3.3	2.76	3.3

Note: η: global hardness; σ: global softness; μ: chemical potential; ω: global electrophilicity index; χ: electronegativity.
Source: Elaborated by the authors.

These results align with experimental insecticidal activity and docking profiles, highlighting **D**, **F**, and **M** as the most reactive and biologically potent compounds. Thus, global descriptors support their potential as selective, non-toxic pest control agents.

Global hardness (η) measures a compound's resistance to deformation of its electron cloud. It is typically associated with molecular stability; compounds with high η values are generally more stable and less reactive. In contrast, global softness (σ), the inverse of hardness, correlates with higher polarizability and molecular flexibility. Soft molecules are chemically reactive and interact more effectively with biological receptors (Erazua and Adeleke, 2024). In this study, compounds **D**, **F**, and **M** exhibited lower hardness values (1.970 -1.995 eV) and higher softness values (~0.501 eV^{-1}), supporting their greater molecular reactivity and stronger interaction with *Rhyzopertha dominica* receptor targets. This theoretical observation aligns with the binding affinities obtained from molecular docking, where **D** and **M** displayed the lowest docking scores and most favourable interactions with key residues.

Chemical potential (μ) describes the escaping tendency of electrons from an equilibrium system and is influenced by the system's electron distribution. A more negative μ value indicates a stronger ability to attract electrons and generally correlates with improved interaction with electrophilic sites of biological targets (Erazua *et al*., 2024). Compounds **D** and **F** recorded the most negative chemical potentials (-3.555 and -0.570 eV, respectively), further affirming their stronger electron-accepting tendencies and binding efficiencies. This is consistent with their docking results and high insecticidal activity observed experimentally.

Electrophilicity index (ω) quantifies a molecule's ability to accept electrons. A higher ω value indicates a greater tendency to undergo electrophilic attack, often resulting in more potent inhibition of biological targets (Erazua and Adeleke, 2019). Compounds **D** and **F** had the highest ω values (~3.200 eV), while compound **K** had the lowest (2.557 eV), mirroring the observed trend in bioactivity. **D** and **F** were among the most active insecticidal agents, whereas **K** showed the least efficacy against *Rhyzopertha dominica*.

Lastly, electronegativity (χ), which reflects a compound's tendency to attract electron density, also enhances receptor-ligand interaction by influencing molecular polarity and charge distribution. The high electronegativity values observed in **D** and

F contributed to stronger non-covalent interactions, such as hydrogen bonding and van der Waals forces, with critical amino acid residues at the receptor site.

These findings reinforce the value of integrating theoretical descriptors with experimental evaluation in the rational design of bioactive agrochemicals.

3.4. Molecular docking studies

In addition to DFT, molecular docking was applied to assess the binding potential of the synthesized compounds with target insect proteins. This technique helps simulate ligand-receptor interactions and predict binding affinities, thereby identifying the molecular basis for biological activity. The experimental outcomes demonstrated that specific Schiff bases have insecticidal properties against *Rhyzopertha dominica.* A comparative analysis was done in silico by docking method using two protein targets to complement the experimental study. Nine conformers were considered for each ligand-enzyme complex, and the conformation with the least binding energy (highest negative value) was identified as the best binding mode of the docked compound to the target enzyme (Erazua *et al.,* 2023). Tables 4 and 5 list the protein residues in the interaction, distance, binding energy, and inhibition constant (*Ki*) for each complex that the investigated compounds and standard generated. Figures 1 and 2 also show the types of interactions and the protein residues implicated.

The 3WE1 receptor complexes that were created showed binding energy between –23.4 to –25.5 kJ/mol (Table 4), with compounds D and M having the lowest binding energy and hence better activity. Conventional hydrogen bonds are observed for all the compounds except compound K. Pi-alkyl and van der Waals forces were noticed for every compound. Pi-sigma interactions were observed for all test compounds except for compound H. Compound D possesses a halogen bond, compound H had a pi-donor hydrogen bond, compound M showed pi-anion, while Compound K showed pi-cation and amide pi-stacked interaction (Fig. 1).

Protein 5BIC was also docked against *Rhyzopertha dominica* and the result showed good interactions (Table 5 and Fig. 2). The observed interactions include conventional hydrogen bonds, pi-alkyl, pi-anion, pi-sigma, pi-cation, pi-donor hydrogen bonds, pi-pi-T-shaped, and Van der Waals forces. The studied compounds exhibited a range of binding affinities from –24.3 to –27.6 kJ/mol. The standard used (permethrin) showed the lowest binding energy, indicating that it has a stronger binding interaction than the Schiff bases. Compound M had the lowest binding energy, (better activities) among the Schiff bases, while compound K had the least inhibition strength against the insect species, as shown in Table 3. This observation agrees with the experimental data.

The docking studies revealed that amino acid residues such as Ser633, Arg619, and Thr634 formed key interactions with the most active ligands. These residues play a vital role in stabilizing ligand binding and enhancing inhibition, as supported by literature on bioactive molecule receptor systems (Erazua *et al*., 2023; Yusuf *et al.*, 2020). Consequently, molecular docking validated the observed experimental trends and provided insight into the mechanistic action of the compounds. The approach facilitated a rational interpretation of structure-activity relationships and highlighted the therapeutic potential of the most active Schiff bases.

Table 4. Binding energy and interactions between ligands and receptor 3WE1.

Compound	Hydrogen interaction		Hydrophobic Interaction	ΔG (kJ/mol)	Ki (μmol/L)	% Mortality
	Residue	Distance (Å)				
D	Ser633	3.58	Thr634, Ser632, Leu636, Glu638, Pro635, Thr644, Asn645.	−25.5	33.75	100
F	Ser632 Asn645	4.20 4.39	Ser633, Ile631, Glu645, Pro635 Leu636, Thr634. Glu638, Thr644u.	−23.4	78.48	100
H	Ile618 Val626	3.41 4.58	Thr634, Ser632, Ile616, Glu617, Arg629, GLY628. Val627, Lys625, Lys613, Ile630, Pro635, Ser633.	−24.3	55.99	70
K	NIL	NIL	GLY628, Val627, Val626, Ile630, Arg629, Ile618, Glu617, Ile-616, Pro635, Lys613, Thr634, Val614.	−25.1	39.95	50
M	Arg619	5.06	Met580, Glu617, Pro615, Gly660, Thr-667, Lys623, Tyr656, Val658, Gly662, Val661, Ala665.	−25.5	33.75	100
Standard	Thr634 Arg629 Gly628	4.50 6.69 3.60	Ile618, Val627, Glu617, Lys625, Lys613, Ile-616. Pro615, Pro635, Met580, Val614, Ile630, Val626. -	−24.3	55.99	100

Source: Elaborated by the authors.

Table 5. Binding energy and interactions between ligands and receptor 5BIC.

Compound	Hydrogen interaction		Hydrophobic Interaction	ΔG (kJ/mol)	Ki (μmol/L)
	Residue	Distance (Å)			
D	Ser351	3.84	Val362, Thr363, Glu357, Leu355, Pro354, Ser352, Asn364, Glu366, Val319.	−25.5	33.75
F	Leu355	3.89	Thr353, Pro354, Glu357, Ser361, Val362, Asn364, Thr363, Ser352.	−25.5	33.75
H	Val345 Lys344	5.06 3.78	Pro334, Lys332, Ile335, Val346, Gly347. Arg348, Ile337, Ile349, Pro354, Thr353, Met299, Val333.	−25.1	39.95
K	NIL	NIL	Lys342, Tyr375, Arg338, Thr386, Val377, Ala384, Glu336, Gly379, Val380, Gly381.	−24.3	55.99
M	Arg338	5.35	Val380, Glu336, Gly379, Lys342, Tyr375, Thr386, Val377, Gly381, Ala384.	−26.8	20.33
Standard	Thr353 Ile349 Arg348	3.57 4.22 5.65	Glu336, Lys344, Val-346, Pro334, Ile335. Val333, Pro354, Thr353, Ser352, Ser351. Gly-347, Ile337, Val-345.	−27.6	14.51

Source: Elaborated by the authors.

https://doi.org/10.26850/1678-4618.eq.v51.2026.e1560

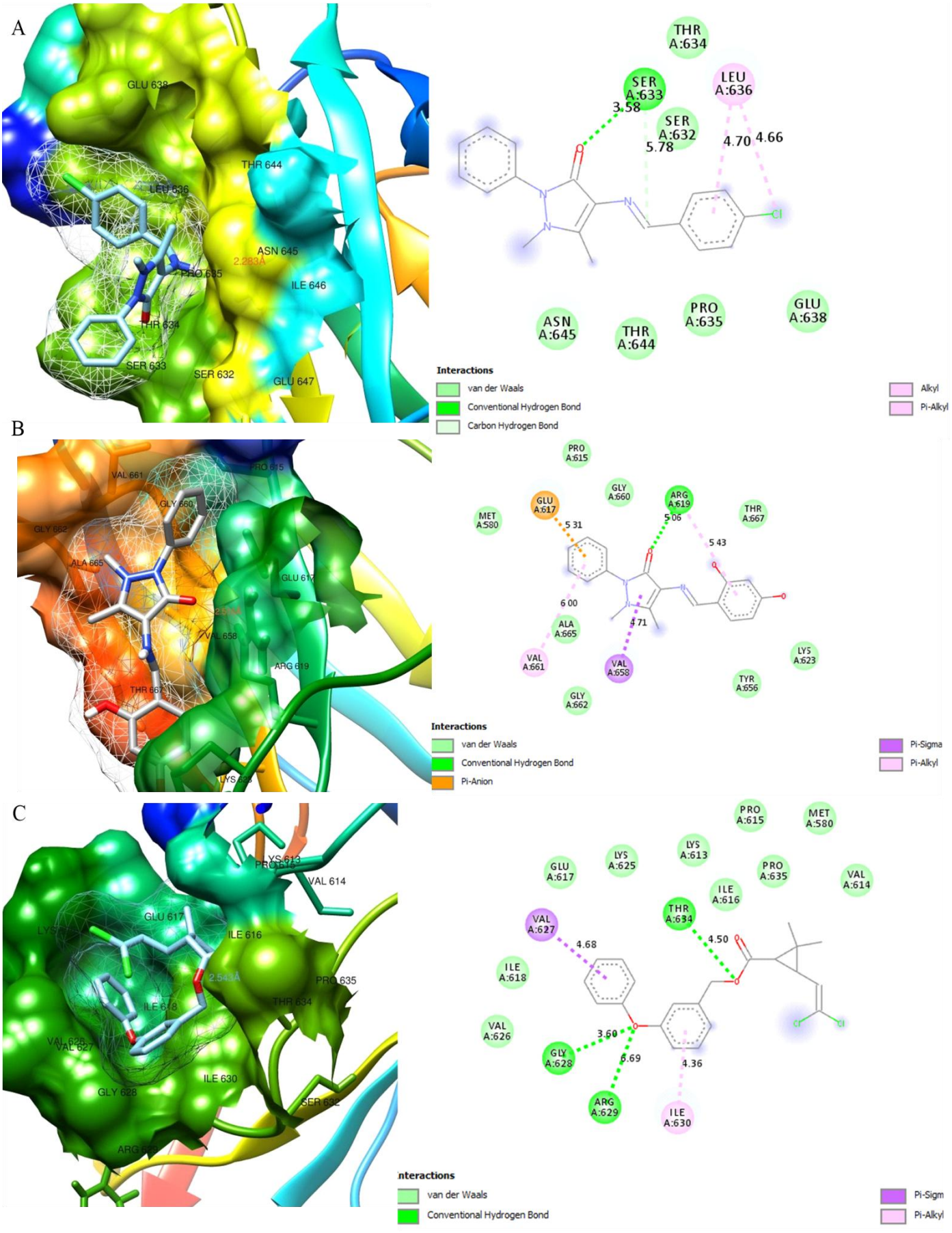

Figure 1. Three-dimensional (left) and two-dimensional (right) images showing the molecular interactions between receptor amino acid residues of 3WE1 with Compounds **(a) D**, **(b) M** and **(c)** Permethrin (standard drug).
Source: Elaborated by the authors.

https://doi.org/10.26850/1678-4618.eq.v51.2026.e1560

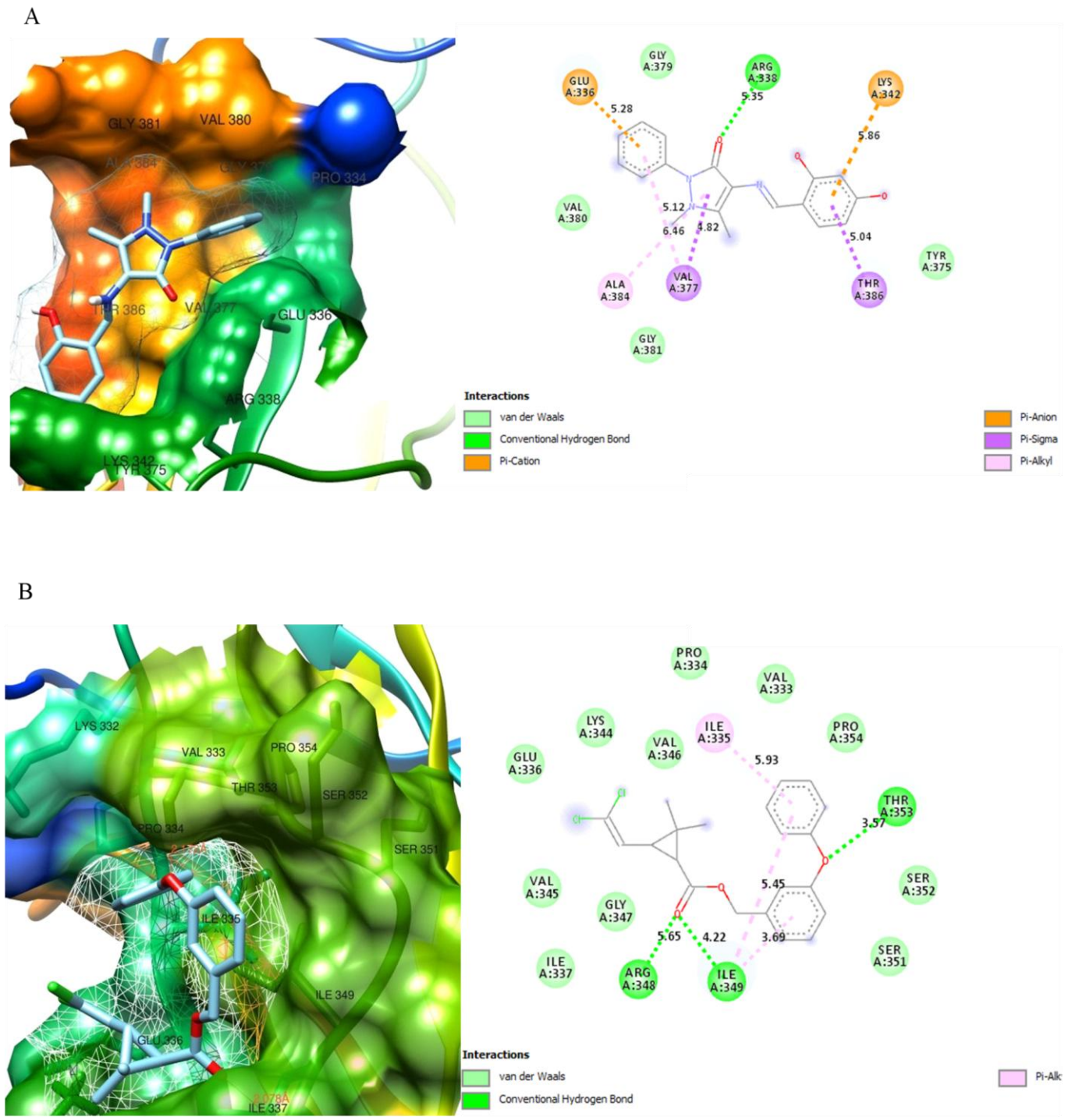

Figure 2. Three-dimensional (left) and two-dimensional (right) images showing the molecular interactions between receptor amino acid residues of 5BIC with compound **(a) M** and **(b)** Permethrin (standard drug).

Source: Elaborated by the authors.

4. Conclusions

In the search for potent insecticides, thirteen (13) Schiff bases were synthesized from 4-amino antipyrine and different substituted benzaldehydes and were characterized with varying techniques of spectroscopy. None of the compounds showed cytotoxicity in *Artemia salina* assays, suggesting good safety profiles. Biological screening against three insect species revealed that five compounds selectively inhibited *Rhyzopertha dominica*, with compounds **D** and **M** showing the highest efficacy, while **K** showed the least. Complementary DFT and molecular docking studies provided insights into the compounds' electronic structure and interaction profiles. Notably, compounds **D**, **F**, and **M** exhibited lower electronic gaps, higher softness, and more negative chemical potential properties aligned with enhanced binding affinity and biological activity. High electrophilicity and electronegativity further supported their strong interactions with key amino acid residues at the receptor binding site. The computational descriptors reinforced the experimental findings, identifying compounds **D** and **M** as promising candidates for selective, non-cytotoxic insecticidal agents. This integrated approach highlights the value of combining theoretical and experimental methods in the rational design of agrochemicals.

Authors' contribution

Conceptualization: Babatunde Benjamin Adeleke; Ehimen Annastasia Erazua. **Data curation**: Ehimen Annastasia Erazua. **Formal Analysis**: Babatunde Benjamin Adeleke; Ehimen Annastasia Erazua. **Funding acquisition**: Babatunde Benjamin Adeleke; Ehimen Annastasia Erazua. **Investigation**: Ehimen Annastasia Erazua. **Methodology**: Ehimen Annastasia Erazua. **Project administration**: Ehimen Annastasia Erazua. **Resources**: Babatunde Benjamin Adeleke; Ehimen Annastasia Erazua. **Software**: Ehimen Annastasia Erazua. **Supervision**: Babatunde Benjamin Adeleke. **Validation**: Babatunde Benjamin Adeleke; Ehimen Annastasia Erazua. **Visualization**: Babatunde Benjamin Adeleke; Ehimen Annastasia Erazua. **Writing – original draft**: Ehimen Annastasia Erazua. **Writing – review & editing**: Babatunde Benjamin Adeleke; Ehimen Annastasia Erazua.

Conflict of interest

The authors declare that there is no conflict of interest.

Data availability statement

All datasets generated or analyzed during the current study are available from the corresponding author upon reasonable request.

Artificial Intelligence usage statement

The authors declare that they did not use Artificial Intelligence tools at any stage of the preparation, correction, or evaluation of this work.

Funding

This research was funded by The World Academy of Science (TWAS) FR number: 3240305617.

Acknowledgments

The authors acknowledge the World Academy of Science for the Award of the 2018 ICCBS-TWAS Sandwich Postgraduate Fellowship awarded to Ms. Erazua Ehimen Annastasia (FR number: 3240305617). We also acknowledge Dr. Hina Siddiqui, and Prof. M. Iqbal Choudhary, at the International Center for Chemical and Biological Sciences University of Karachi, Pakistan where the fellowship was tenable.

References

Akbari, Z.; Stagno, C.; Iraci, N.; Efferth, T.; Omer, E. A.; Piperno, A.; Micale, N. Biological evaluation, DFT, MEP, HOMO-LUMO analysis and ensemble docking studies of Zn (II) complexes of bidentate and tetradentate Schiff base ligands as antileukemia agents. *Journal of Molecular Structure*, **2024**, 1301, 137400. https://doi.org/10.1016/j.molstruc.2023.137400

Banti, C. N.; Hadjikakou, S. K. Evaluation of Toxicity with Brine Shrimp Assay. *Bio-prot.* **2021**, *11* (2), e3895. https://doi.org/10.21769/BioProtoc.3895

Becke, A. D. Density-functional thermochemistry. III. The role of exact exchange. *J. Chem. Phys.* **1993**, *98*, 5648–5652. https://doi.org/10.1063/1.464913

Dissanayaka, D. M. S. K.; Sammani, A. M. P.; Wijayaratne, L. K. W.; Rajapakse, R. H. S.; Hettiarachchi, S, Morrison W. R. Effects of aggregation pheromone concentration and distance on the trapping of *Rhyzopertha dominica* (Coleoptera: Bostrychidae) adults. *J. Stored. Prod. Res.* **2020**, *88*, 1–10. https://doi.org/10.1016/j.jspr.2020.101657

Erazua, E. A.; Adeleke, B. B. DFT and Molecular Docking Investigation of Potential Anticancer Properties of Some Flavonoids. *J. Pure Appl. Chem.* **2019**, *8* (3), 225–231. https://doi.org/10.21776/ub.jpacr.2019.008.03.485

Erazua, E. A.; Oyebamiji, A. K.; Adeleke, B. B. DFT-QSAR and Molecular Docking Studies on 1,2,3-Triazole-Dithiocarbamate Hybrids as Potential Anticancer Agents. *Phys. Sci. Int.* **2019**, *4*, 1–10. https://doi.org/10.26538/tjnpr/v5i11.22

Erazua, E. A.; Adepoju, A. J.; Ajayi, A. P.; Josiah, O. M.; Akintelu, S. A; Oyebamiji, A. K. Theoretical Studies on Triazoles of 3-Acetylbetulin and Betulone as Anticancer Agents. *Nat and Sci.* **2021**, *19* (7), 5–18. https://doi.org/10.7537/marsnsj190721.02

Erazua, E. A.; Oyebamiji, A. K.; Akintelu, S. A.; Adewole, P. D.; Adelakun, A.; Adeleke, B. B. Quantitative Structure-Activity relationship, Molecular Docking and ADMET Screening of Tetrahydroquinoline Derivatives as Anti-Small Cell Lung Cancer Agents. *Eclét. Quím*. **2023**, *48* (1), 55–71. https://doi.org/10.26850/1678-4618eqj.v48.1.2023.p55-71

Erazua, E. A.; Adeleke, B. B. Antioxidant, anti-inflammatory and anti-glycation activities of some 4-aminoantypyrine derivatives: In vitro and in silico study. *JOPAT*. **2024**, *23* (1), 1313–1347. https://doi.org/10.4314/jopat.v23i1.9

Erazua, E. A; Olaseinde, A. A; Oyebamiji, A. K; Oluwakemi, E.; Adekunle, D.; Olanrewaju, A. A. Molecular docking and ADMET profiling of Carbazole-rhodanine hybrid as anticancer agent. *JOPAT*. **2024**, *23* (2), 1491–1515. https://doi.org/10.4314/jopat.v23i2.8

Gareau, B. J. Lessons from the Montreal Protocol delay in phasing out methyl bromide. *J. Environ. Sci. Stud.* **2015**, *5* (2), 163–168. https://doi.org/10.1007/s13412-014-0212-x

Ghorab, M. M.; El-Gazzar, M. G.; Alsaid, M. S. Synthesis, Characterization and Anti-Breast Cancer Activity of New 4-Aminoantipyrine-Based Heterocycles. *Int. J. Mol. Sci.* **2014**, *15*, 539–553. https://doi.org/10.3390/ijms15057539

Grewal, A. S.; Singla, A.; Kamboj, P.; Dua, J. S.; Pesticide residues in food grains, vegetables, and fruits: a hazard to human health. *J. Med. Chem. and Tox.* **2017**, *2* (1), 40–46. https://doi.org/10.15436/2575-808X.17.1355

Halim, K. N. M.; Ramadan, S. K.; Rizk, S. A.; El-Hashash, M. A. Synthesis, DFT study, molecular docking, and insecticidal evaluation of some pyrazole-based tetrahydropyramimidine derivatives. *Synth. Commun.* **2020**, *50* (8), 1159–1175. https://doi.org/10.1080/00397911.2020.1720739

Herrera, J. M.; Pizzolitto, R. P.; Zunino, M. P, Dambolena, J. S.; Zygadlo, J. A. Effect of fungal volatile organic compounds on a fungus and an insect that damage stored maize. *J Stored Prod Res.* **2015**, *62*, 74–80. https://doi.org/10.1016/j.jspr.2015.04.006

Huang, D.; Liu, A.; Liu, W.; Liu, X.; Ren, Y.; Zheng, X. Synthesis and insecticidal activities of novel 1*H*-pyrazole-5-carboxylic acid derivatives. *Heterocycl Commun*. **2012**, *23* (6), 455–460. https://doi.org/10.1515/hc-2017-0110

Kashyap, S.; Kumar, S.; Ramasamy, K.; Lim, S. M.; Shah, S. A; Narasimhan, B. Synthesis, biological evaluation, and corrosion inhibition studies of transition metal complexes of Schiff base. *Chem. Cent. J.* **2018**, *12*, 117. https://doi.org/10.1186/s13065-018-0487-1

Kaya, K.Y.; Yilmaz, V. T.; and Buyukgungor, O. Synthesis, Spectroscopic, Structural and Quantum Chemical Studies of a New Imine Oxime and Its Palladium (II) Complex: Hydrolysis Mechanism. *Molecules.* **2016**, *21* (1), 52. https://doi.org/10.3390/molecules21010052

Khan, S. A.; Ranjha, M. H.; Khan, A. A; Sagheer, M.; Abbas, A.; Hassan, Z.; Insecticidal efficacy of wild medicinal plants, *Dhutura alba* and *Calotropis procera*, against *Trogoderma granarium* (Everts) in wheat store grains. *Pak. J. Zoo*. **2019**, *51* (1), 289–294. https://doi.org/10.17582/journal.pjz/2019.51.1.289.294

Kim, M.; Sim, C.; Shin, D.; Suh, E.; Cho, K. Residual and Sublethal Effects of Fenpyroximate and Pyridaben on the Instantaneous Rate of Increase of Tetranychus Urticae. *Crop Prot.* **2006**, *25*, 542–548. https://doi.org/10.1016/j.cropro.2005.08.010

Lampiri, E.; Agrafioti, P; Levizou, E.; Athanassiou, C. G.; Insecticidal effect of *Dittrichia* viscosa lyophilized epicuticular material against four major stored-product beetle species on wheat. *Crop Prot.* **2019**, *132*, 105–119. https://doi.org/10.1016/j.cropro.2020.105095

Marcic, D. Sublethal Effects of Tebufenpyrad on the Eggs and Immatures of Two-Spotted Spider Mite, Tetranychus Urticae. *Exp. Appl. Acarol*. **2005**, *36*, 177–185. https://doi.org/10.1007/s10493-005-3579-2

Matsuzaka, Y.; Uesawa, Y. Computational Models That Use a Quantitative Structure-Activity Relationship Approach Based on Deep Learning. *Processes.* **2023**, *11*, 1296. https://doi.org/10.3390/pr11041296

Murtaza, S.; Akhtar, M. S.; Kanwal, F.; Abbas, A.; Ashiq S.; Shamim S. Synthesis and biological evaluation of schiff bases of 4-aminophenazone as anti-inflammatory, analgesic and antipyretic agent. *J. Saudi Chem. Soc*. **2017**, *21*, S359–S372. https://doi.org/10.1016/j.jscs.2014.04.003

Neggaz, S.; Chenni, M.; Zitouni-Haouar, F. E.; Fernandez, X. Mycochemical composition and insecticidal bioactivity of Algerian desert truffles extract against two stored-product insects: *Sitophilus oryzae* (L.) (Coleoptera: Curculionidae) and *Rhyzopertha dominica* (F.) (Coleoptera: Bostrychidae). *Biotech.* **2010**, *10* (11), 481. https://doi.org/10.1007/s13205-020-02472-2

Nonaka, N. Tolfenpyrad-A New Insecticide with Wide Spectrum and Unique Action. *Agrochem Jpn.* **2003**, *83*, 17–19.

Nopsa, J. F. H.; Daglish, G. J.; Hagstrum, D. W.; Leslie, J. F.; Phillips, T. W.; Scoglio, C.; Thomas-Sharma, S.; Walter, G. H.; Garret, K. A. Ecological Networks in Stored Grain: Key Postharvest Nodes for Emerging Pests, Pathogens, and Mycotoxins. *Biosci*. **2015**, *65*, 985–1002. https://doi.org/10.1093/biosci/biv122

Oyebamiji, K. A.; Semire, B. Studies of 1, 4-Dihydropyridine Derivatives for Anti-Breast Cancer (MCF-7) Activities: Combinations of DFT-QSAR and Docking Methods. *N. Y. Sci. J.* **2016**, *9* (6), 58–66. https://doi.org/10.7537/marsnys09061610

Raman, N.; Selvan, A.; Manisankar, P. Spectral, magnetic, biocidal screening, DNA binding and photocleavage studies of mononuclear Cu (II) and Zn (II) metal complexes of tricoordinate heterocyclic Schiff base ligands of pyrazolone and semicarbazide/thiosemicarbazide based derivatives. *Spectrochim. Acta – A*. **2017**, *76*, 161–173. https://doi.org/10.1016/j.saa.2010.03.007

Raza, M.A.; Mumtaz, M.W.; Ozturk, S.; Latif, M.; Aisha; Ashraf, A.; Dege, N.; Dogan, O.E.; Agar, E.; Rehman, S.U.; et al. Experimental and Theoretical Biological Probing of Schiff Bases as Esterase Inhibitors: Structural, Spectral and Molecular Insights. *Molecules* **2023**, *28*, 5703. https://doi.org/10.3390/molecules28155703

Rouhani, M.; Samih, M.A.; Gorji, M.; Moradi, B. H. Insecticidal effect of plant extracts on common *Pistachio psylla*, *Agonoscena pistaciae* Burckhardt and lauterer (Hemiptera: Aphalaridae). *Arch. Phytopathol. Plant Prot*. **2019**, *52* (1–2), 45–53. https://doi.org/10.1080/03235408.2019.1570589

Sabaa, M. W.; Mohamed, N. A; Mohamed, R. R.; Khalil, K. M.; Latif, S. M. Synthesis, Characterization and Antimicrobial Activity of Poly (N-Vinyl imidazole) Grafted Carboxymethyl Chitosan. *Carbohydr. Polym.* **2010**, *79*, 998–1005. https://doi.org/10.1016/j.carbpol.2009.10.024

Selby, T. P.; Lahm, G. P.; Stevenson, T. M.; Hughes, K. A; Cordova, D; Annan, I. B. Discovery of Cyantraniliprole, a Potent and Selective Anthranilic Diamide Ryanodine Receptor Activator with Cross-Spectrum Insecticidal Activity. *Bioorg. Med. Chem. Lett*. **2013**, *23*, 6341–6345. https://doi.org/10.1016/j.bmcl.2013.09.076

Singh, G.; Satija, P.; Singh, B.; Sinha, S.; Sehgal, R.; Sahoo, S. C. Design, crystal structures and sustainable synthesis of family of antipyrine derivatives: Abolish to bacterial and parasitic infection. *J. Mol. Struct.* **2020**, *1199*, 127010. https://doi.org/10.1016/j.molstruc.2019.127010

Song, H.; Liu, Y.; Xiong, L.; Li, Y.; Yang, N.; Wang, Q. Design, Synthesis, and Insecticidal Activity of Novel Pyrazole Derivatives Containing α-Hydroxymethyl-N-benzyl Carboxamide, α-Chloromethyl-N-benzyl Carboxamide, and 4,5-Dihydrooxazole Moieties. *J. Agric. Food Chem.* **2012**, *60*, 1470–1479. https://doi.org/10.1021/jf204778v

Suryawanshi, V. S.; Yadav, A. R; Mohite, S. K.; Magdum, C. S. Toxicological Assessment using Brine Shrimp Lethality Assay and Antimicrobial activity of Capparis Grandis. *Shanghai Ligong Daxue Xuebao.* **2020**, *22* (11), 746–759.

Suthisut, D.; Fields, P. G.; Chandrapatya, A. Fumigant toxicity of essential oils from three Thai plants (Zingiberaceae) and their major compounds against *Sitophilus zeamais*, *Tribolium castaneum* and two parasitoids. *J Stored Prod Res.* **2011**, *47*, 222–230. https://doi.org/10.1016/j.jspr.2011.03.002

Teran, R.; Guevara, R.; Mora, J.; Dobronski, L.; Barreiro-Costa, O; Beske. Characterization of Antimicrobial, Antioxidant, and Leishmanicidal Activities of Schiff Base Derivatives of 4-Aminoantipyrine. *Mol.* **2019**, *24* (15), 2696. https://doi.org/10.3390/molecules24152696

Trott, O.; Olson, A. J; AutoDock Vina: Improving the Speed and Accuracy of Docking with a New Scoring Function, Efficient Optimization and Multithreading. *J. Comput. Chem*. **2010**, *31*, 455–461. https://doi.org/10.1002/jcc.21334

Yaman, C.; Simsek, S. Insecticidal effect from three *Hypericum* species extracts against *Rhyzopertha dominica*, *Sitophilus oryzae* and *Tribolium confusum*. *Ciência e Agrotecnologia.* **2021**, *45*, e001921. https://doi.org/10.1590/1413-7054202145001921

Yang, L.; Feng, J.; Ren, A. Theoretical studies on the electronic and optical properties of two thiophene–fluorene based π-conjugated copolymers. *Polym. J.* **2005**, *46*, 10970–10982. https://doi.org/10.1016/j.polymer.2005.09.050

Yu, H.; Xu, M.; Cheng, Y.; Wu, H.; Luo, Y.; Li, B. Synthesis and Acaricidal Activity of Cyenopyrafen and Its Geometric Isomer. *Arkivoc.* **2012**, *VI*, 26–34. https://doi.org/10.3998/ark.5550190.0013.603

Yusuf, T. L.; Oladipo, S. D.; Olagboye, S. A; Zamisa, S. J.; Tolufashe, G. F. Solvent-free synthesis of nitrobenzyl Schiff bases: Characterization, antibacterial studies, density functional theory and molecular docking studies. *Journal of Molecular Structure.* **2020,** 1222: 128857. https://doi.org/10.1016/j.molstruc.2020.128857

Zaater, S.; Bouchoucha, A.; Djebbar, S.; Brahimi, M. Structure, vibrational analysis, electronic properties, and chemical reactivity of two benzoxazole derivatives: functional density theory study. *J. Mol. Struct*. **2016**, *1123*, 344–354. https://doi.org/10.1016/j.molstruc.2016.06.047